Tidal flow over a sill in Muchalat Inlet, Nootka Sound, and the resultant mixing processes

Senior Thesis

31 May 2015

Jemima Rama

University of Washington

School of Oceanography

ramaj@uw.edu

Acknowledgements

I would like to thank the crew and students who participated in the UW senior cruise 2014 and helped in the acquisition of the data. I would also like to thank Charles Eriksen for his continuous guidance and Arthur Nowell for his support and help in writing this paper.

Abstract:

The tidal flow over Williamson Sill, situated in Nootka Sound, is analyzed by reviewing the changes in the density and velocity field across the sill and over the tidal cycle. The density is calculated from the raw data collected by UCTD casts while the velocity data was acquired from the ADCP. It was determined that the tidal forcing over the sill followed the 'internal lee waves' mechanism as opposed to the 'stationary lee depression' mechanism. During the first half cycle of ebb/flood, the lee waves were generated and held stationary downstream of the sill. These waves then propagated upstream when the tidal current started to wane. The interference of a propagating unsteady lee wave with a newly formed lee wave over the sill can cause wave breaking and substantial mixing.

Introduction

Water exchange and flow processes in fjords prove to be interesting fields of study. Unlike the deep ocean, fjords are easily accessible and hence can serve as proxy for strong tidal flows over large amplitude sills or submarine ridges. The main disparity between these two oceanographic environments is that the stratification in fjords is more significant due to the continuous freshwater discharge from rivers.

Focusing on fjords, there are several mechanisms that allow the exchange of water across the sills but the two common mechanisms are meteorological forcing that a creates horizontal pressure gradient across the sills and barotropic effects, namely tidal action that forces cyclic exchange of water over the sill (Vlasenko et al. 2002). Depending on the bathymetry of the sill, the speed of the tidal currents and the degree of stratification of the water column, the oscillatory tidal flow over the sill generates two different processes with associated sets of features (Cummins et al. 2003).

Farmer and Armi (1999) conducted a study in the fjords of Knight Inlet, British Columbia and characterized the ebbing tidal flow, provided that the water column is stratified, as one which bifurcates on the lee side when the tidal currents increase (Figure 1). As the tide is ebbing, denser seawater diverges from the lighter fresh water and plunges downstream of the sill's crest. An intermediate layer resides downstream of the bifurcation separating the active deep accelerating flow and the passive surface layer, which in this case is the fresh riverine discharge. The shear interface between the accelerated jet and the overlying stagnant fluid is highly unstable; these instabilities result in small scale eddies and entrainment. Consequently, these factors contribute

towards mixing and hence allows the expansion of the mixed intermediate water mass. It is also important to note that the massive lee depression, produced by the plunging jet, remains nearly stationary and adjusts continuously as the tidal flow relaxes. The mixed layer is thick enough to allow a fully established hydraulically controlled flow. (Cummins et al. 2003).

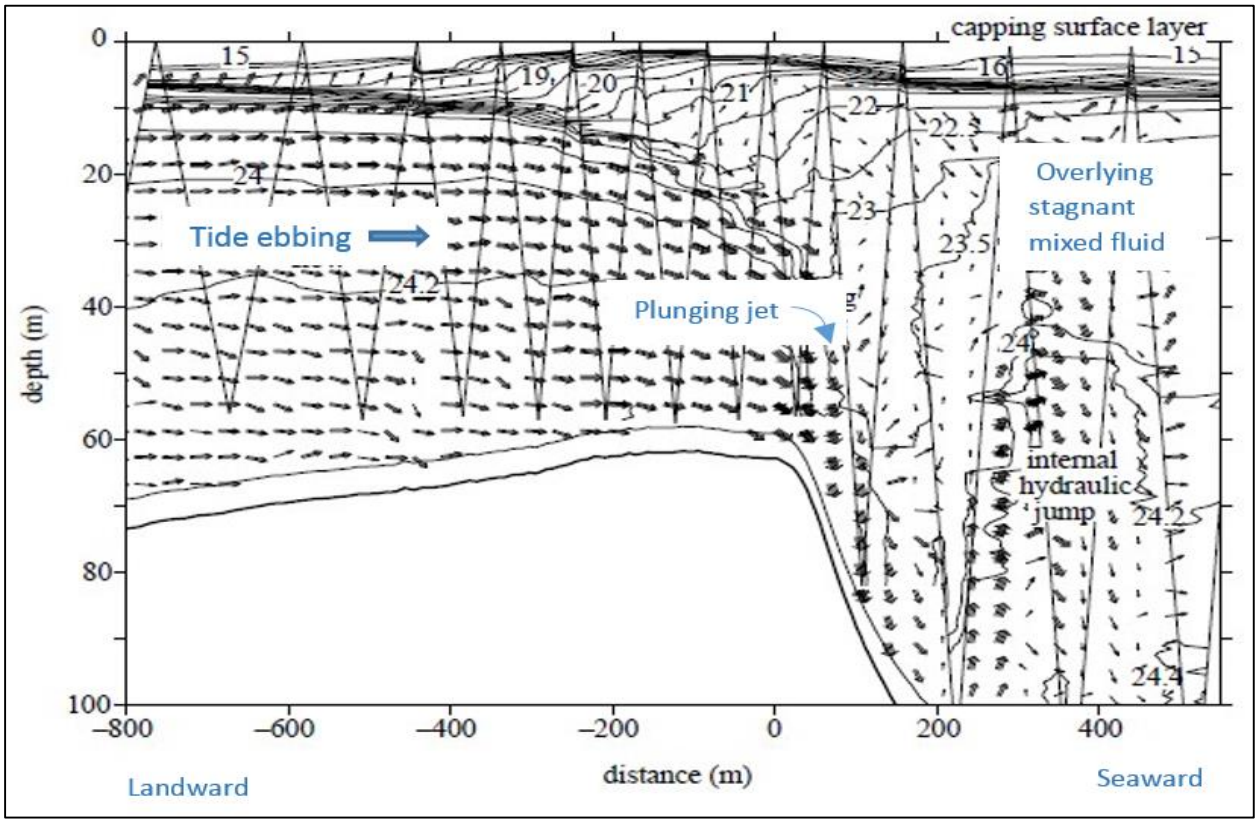

Figure 1: The different features formed when the tidal ebb interact with the sill as explained by Farmer and Armi, (1999)

On the other hand, the most common phenomenon resulting from the interaction of the tidal flow with an underwater sill is the generation of internal waves (or internal tides) close to the area of topographic interaction (Vlasenko et al. 2002). A tidal flow over an obstacle produces vertical currents whose fluctuations in time excite internal waves (Nakamura et al. 2000). As the tidal flow increases over the sill, internal waves (internal lee waves in this case) form progressively on the sill's downstream side and remain trapped at this location for the first half cycle of flood (ebb). While being held motionless, the lee waves extract energy from the increasing barotropic

tidal flow to raise their amplitude and consequently phase speed. Towards the end of the flood (ebb), as the tidal flow starts to wane away, the lee waves whose phase speed were tuned to the maximum tidal current, are now able to propagate upstream, against the tidal current. Lee waves cannot propagate downstream unless they are carried away from their generation site by the tidal flow which then reverses to ebb (flood), (Vlasenko et al. 2002). Moreover, the interference of a propagating unsteady lee wave with a newly formed lee wave over the sill can cause wave breaking and substantial mixing (da Silva et al. 2015).

The study of the intensity of mixing within any oceanic area, including fjords and sills helps in interpreting other oceanographic processes and phenomenon, either chemical, geological or biological. For instance the intensity of mixing controls the turbidity of the water column. Water with high turbidity will inhibit the penetration of light and hence reduce primary production for example. Turbulence also affects the resuspension/ deposition of sediments and consequently maintains the morphology of sills when considering fjords areas (Pickrill 1987). Mixing can also play an essential role in bringing back remineralized nutrients (small organic or inorganic particles) to the surface again for primary production. This scenario is more important in relatively deep fjords with depths exceeding the euphotic zone in winter. In addition to primary producers vertically migrating zooplankton also benefit from these mixing events; they use the tidal flows and entraining eddies to find new foraging areas, escape predators and for hatching of their eggs in nutrient rich surface waters (Castro et al. 2010). Lastly mixing at the sills, controls the buoyancy of the water mass entering the fjord at each tidal cycle. This subsequently determines if the water mass entering the fjord is dense enough to sink and replace the even denser saltier water mass dwelling at the bottom. (Isachsen and Pond, 2000). Ultimately

the mixing events at the sill controls the replacement and circulation of water within the fjords; the difference is chiefly noted between the spring and neap cycle.

Given all the above mentioned points, the analysis of the intensity of mixing proves to be a vital area of study, especially when considering water circulation and exchanges in fjord. This study first attempts to characterize the tidal flow mechanism (either ‘plunging jet’ or ‘lee wave’) and thereafter discuss the mixing events, happening as a result of tidal intrusion over Williamson sill. Williamson sill is situated on the west coast of Vancouver Island, British Columbia, more precisely in Muchalat Inlet and North of Gore Island in Nootka Sound. This site was chosen because it experiences a tidal diurnal cycle and also because the water column in the inlets of Nootka Sound can be considered as stratified. The freshwater input dominates in winter (Nootka Coastal land use plan, 2001) providing fresh less dense water at the surface. As mentioned earlier, these factors are crucial for the formation of either the ‘plunging jet’ or the ‘internal lee waves’, both of which are important components necessary for mixing at Williamson Sill.

The ultimate aim of this study is to first characterize the nature of the barotropic tidal flow over Williamson Sill and therefore state which of the ‘plunging jet’ or ‘internal lee waves’ mechanism holds true in this case. This paper also analyses the mixing events that occur as a result of the above mentioned phenomenon and attempt to determine if there is any temporal variation in the intensity of mixing, over the tidal cycle, at Williamson sill.

Methods

Study area

As mentioned earlier Williamson Sill is situated in Muchalat Inlet, Nootka Sound. The Inlet is fed by Gold River at its head and has two main sills; an outer sill at the entrance of the inlet, west of Gore Island and an inner sill, north of the island. Williamson Sill is the sill north of the Gore Island as shown below in Figure 2. The sill crest is at approximately 70m depth and the adjacent fjord at about 210m. In order to collect the required data, the R/V Thomas Thompson spent 13 hours at Williamson Sill on the 15/16th of December 2014; the locations for data acquisition are shown in Figure 2 below.

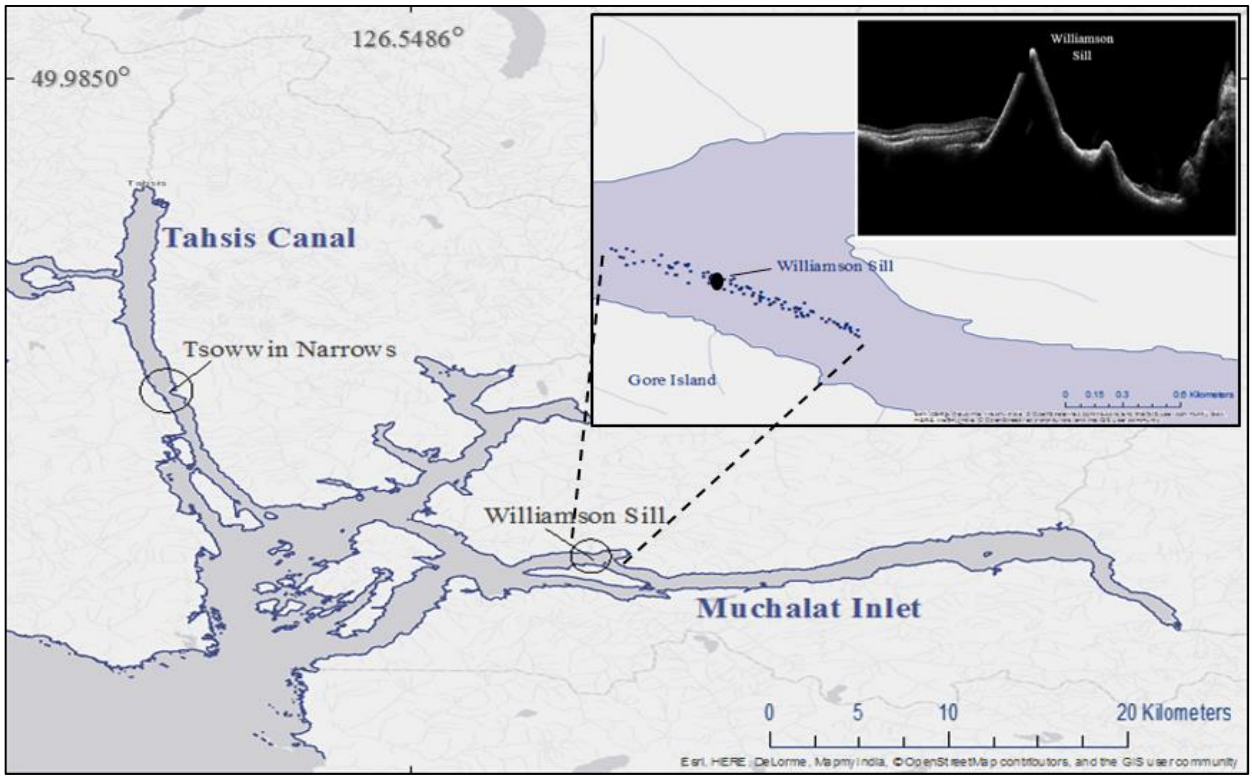

Figure2: Map showing sill locations. Upper left box shows the sampling points at Williamson Sill and its corresponding bathymetry from the sub- bottom profiler backscatter image.

Fieldwork

The main objective during the field observation was to obtain the density field within the water column using the Oceanscience UnderwayCTD (UCTD); a freefall profiler that allows the

acquisition of salinity and temperature profiles of the water column as the ship is moving away from the deployment location. In addition, measurements of the current field within the water column, at different times over the tidal phase were obtained using the ship's hull mounted 75kHz Acoustic Doppler Current profiler (ADCP). At Williamson Sill, the vessel performed repeated back and forth longitudinal transects over the sill crest (24 transects were recorded in 13 hours) at a speed of 6 knots covering the upstream and downstream area approximately 2km away from the sill's crest.

UCTD and density field

During these transects, the UCTD was continuously dropped and winched back up to the surface so as to collect density profiles at different locations and over different phases of the tide, where the tidal height was recorded by pressure gauges deployed further upstream of Muchalat Inlet. Following the test cruise performed on the RV Thompson before the field observations, it was established that the UCTD has a falling rate of 4m/s when the ship is moving at 6 knots. Therefore when deploying the UCTD, the time span during which the UCTD was wired out was calculated by using the water depth, given by the Knudsen 3260 Chirp Echosounder onboard the ship, and the probe's falling rate. It is important to note that as a security measure 20m was subtracted from the actual water depth when calculating the dropping time. This was done so as avoid any collision of the UCTD with the seafloor. However, this also represents a limitation since the UCTD data does not cover the area 20m above the seabed.

Furthermore, the UCTD collects only temperature, conductivity and pressure measurements with the associated time. The temperature and conductivity measurements were crosschecked with the data acquired from the CTD casts deployed near Williamson Sill and the UCTD measurements were corrected for any offset due to the instrument's drift when necessary. The

density field was thereafter computed on Matlab using the above mentioned data and the routines of Seawater Software packages (TEOS-10). It is important to note that the density values within the water column were binned to 1 meter interval vertically. On the other hand, since the UCTD does not record its exact position, the time given by the UCTD was correlated with the ship's navigation time so as to obtain the exact latitude and longitude of the individual UCTD casts.

In addition, from the processed density field, the vertical displacement (η) of the isopycnals over the whole water column was computed for each cast. Isopycnals displacement in the ocean have contributions from turbulence or internal waves and hence can give a good approximation of mixing or indicate the presence of internal waves.

Vertical displacement, $\eta = z - Z_o(\sigma_t)$

The displacement is the depth offset of the isopycnal from the depth at which it lies on the average density profile $Z_o(\sigma_t)$.

ADCP and velocity field

The ship's hull mounted ADCP was recording the flow velocities within the water column throughout the whole duration of the field observation. The ADCP onboard the ship recorded velocity data every 5 minutes, with the vertical resolution (vertical binning) set to 8m. The ADCP did not record any velocity data at depths shallower than 35m, implying that there was no measurement of the surface currents. Furthermore, due to the sidelobe interference of the sloping beams, it seems

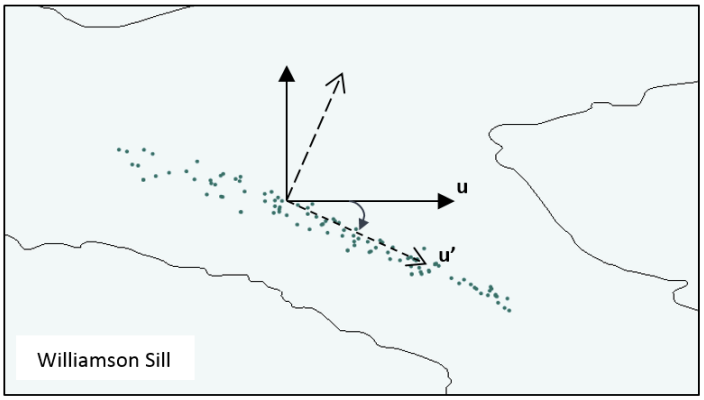

Figure 3: UCTD casts taken along the transects over each sill and the plane of rotation taken for calculation of u' and v'.

that the ADCP does not record accurate velocity data for the bottom 6% of the water column. The CODAS ADCP processing software was thereafter used on Matlab to filter, average out and interpolate (projected to every 1 minute) the acquired data. In order to simplify analysis of the data, only along fjord tidal flow was considered. Given that the transects for Williamson Sill was nearly on the East-West axis, the current velocity in the x- plane prevails (u') and was only accounted for. As shown in Figure 3, the current velocity field (u) given by the ADCP measurements, was rotated to the appropriate angle on the Cartesian plane and u' was computed.

Richardson Number

The different flow velocities and density field processed by Matlab were then used for numerical calculations that characterize the nature of the flows within the water column at each of the UCTD casts along the ship transects. For instance, the Richardson number (Ri) is computed to determine the stability of the flow and hence identify regions that are favorable to the growth of small scale instabilities.

$$R_i = \frac{gN}{\left(\frac{\partial u}{\partial z}\right)^2}$$

g is the gravitational acceleration

$\left(\frac{\partial u}{\partial z}\right)$ is the change in flow velocity with depth

N is the buoyancy frequency where $N = \sqrt{-\frac{1}{\rho}\left(\frac{\partial \rho}{\partial z}\right)}$ and is computed using the Seawater Software package (TEOS-10) in matlab

If Ri > 0.25 the flow is stable but if Ri < 0.25 the flow is unstable and there is high a probability of overturning of water (Isachsen and Pond, 1999). Given that the ADCP vertically binned the velocity data to 8m, Ri was calculated for 8m vertical resolution at each location where a UCTD cast was taken. Due to the ADCP limitation, no Ri was calculated at depths shallower than 35m.

Results

The vertical profiles of temperature, salinity, density (σ_t) and buoyancy frequency (Figure 1) were computed from the averages of all the UCTD casts taken during the transects over Williamson Sill. Considering Figure 4(a), there is a temperature inversion and maxima at about 50m depth, while the salinity (Figure 4(b)) decreases with depth through a 'step-like' halocline that extends down to 70m depth. The density (Figure 4(c)) follows the same 'step-like' profile, separating the water column into 3 distinct layers; the well stratified surface, the modestly stratified intermediate layer (10m-60m) and the relatively well mixed bottom layer. The buoyancy frequency (Figure 4(d), decreases with depth but slightly peaks at 65m depth. Hence the water column bears two strongly stratified layers, one at the surface due to the halocline and a weaker one at 65m depth due to the thermocline.

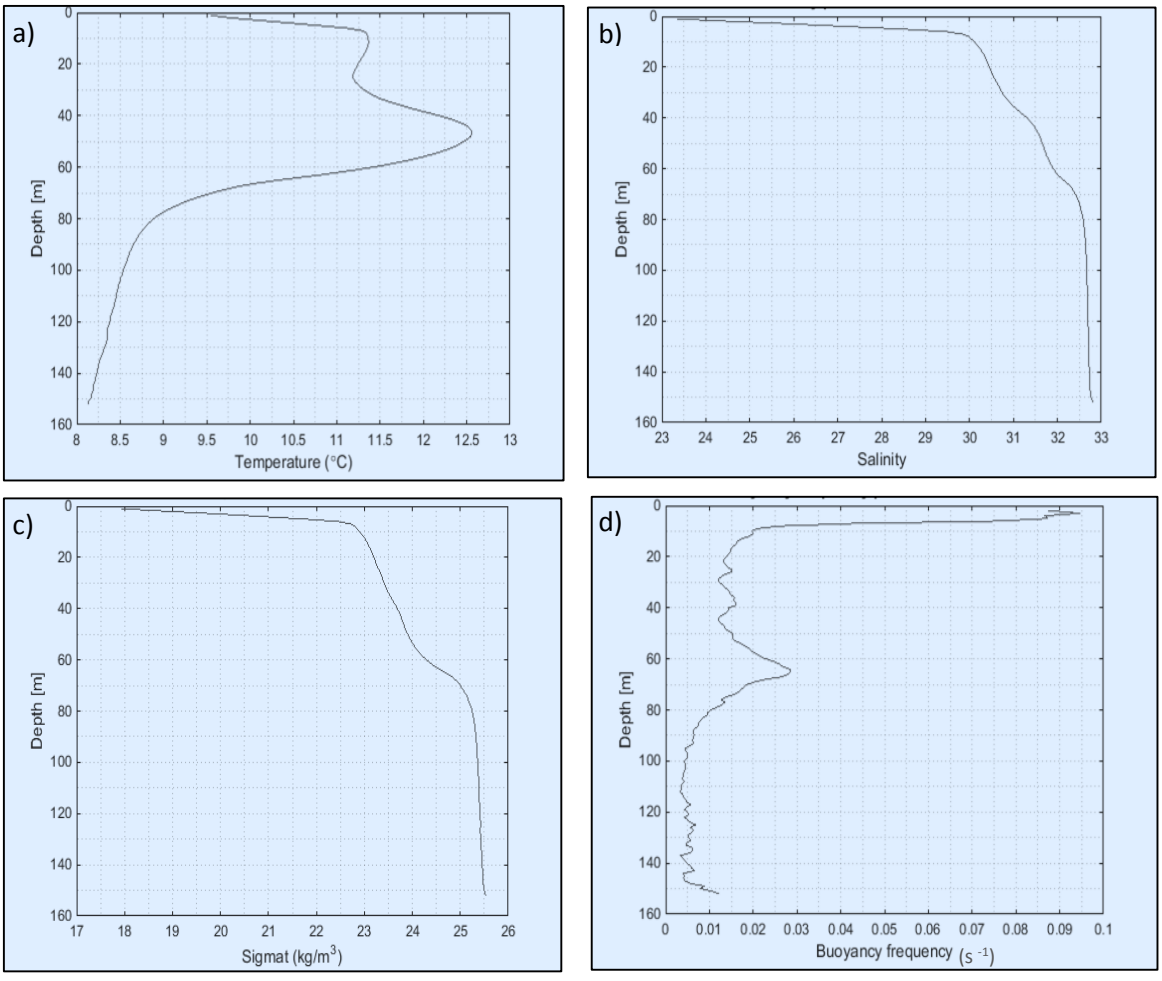

Figure 4: Vertical profiles over Williamson Sill. a) Temperature, b) Salinity, c) Density (σ_t) and d) Buoyancy Frequency (N)

The density field acquired through the UCTD casts and processed using Matlab is used to plot isopycnals, more precisely contours of σ_t $(\sigma_t = \rho(S_{(Z)}, T_{(Z)}, P_{(Z=0)}) - 1000)$ $[kgm^{-3}]$. These isopycnals are overlaid on top of the velocity field from the ADCP data. The different plots (Figure 5) show the same section of the Williamson Sill but for different ship's traverse, that is over different times of the tidal phase (at slack, ebb and flood). The exact time over the tidal cycle is indicated by a red dot in the tidal chart subplot of each figure. The zero on the x-axis represents the highest point of the sill and the x is positive up-fjord and the negative seaward, as shown on each of the plots. The bathymetry represented on the plots was acquired through the processed data of the the Multibeam Echo Sounder. From the 1019kgm^{-3} to 1023 kgm^{-3} isopycnal, the density interval is set to σ_t =1kgm^{-3} while for isopycnals greater than 1023 kgm^{-3}, the interval is specified as σ_t =0.1kgm^{-3}.

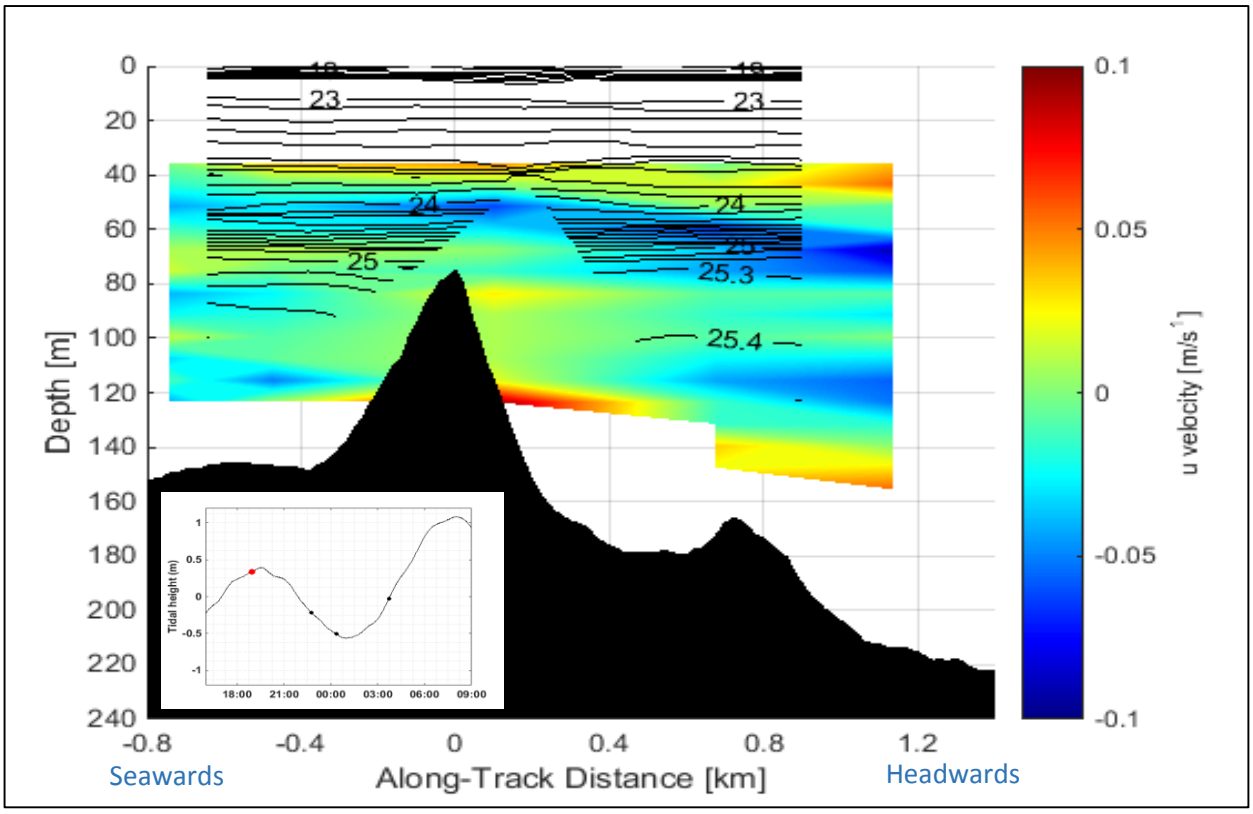

Figure 5(a): Williamson sill at slack water before ebb. The contour plot represents the velocity while the contour lines represent σ_t

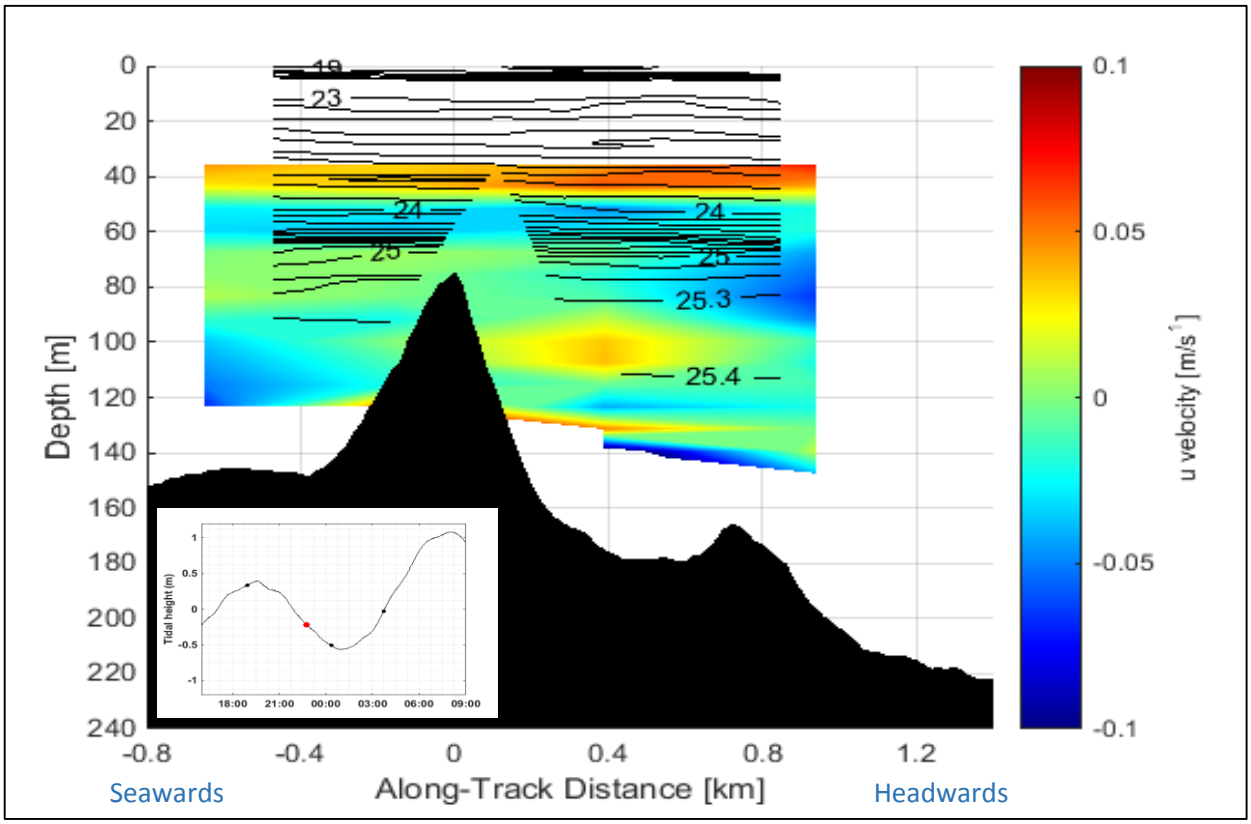

Figure 5(b): Williamson sill during ebb. The contour plot represents the velocity while the contour lines represent σ_t

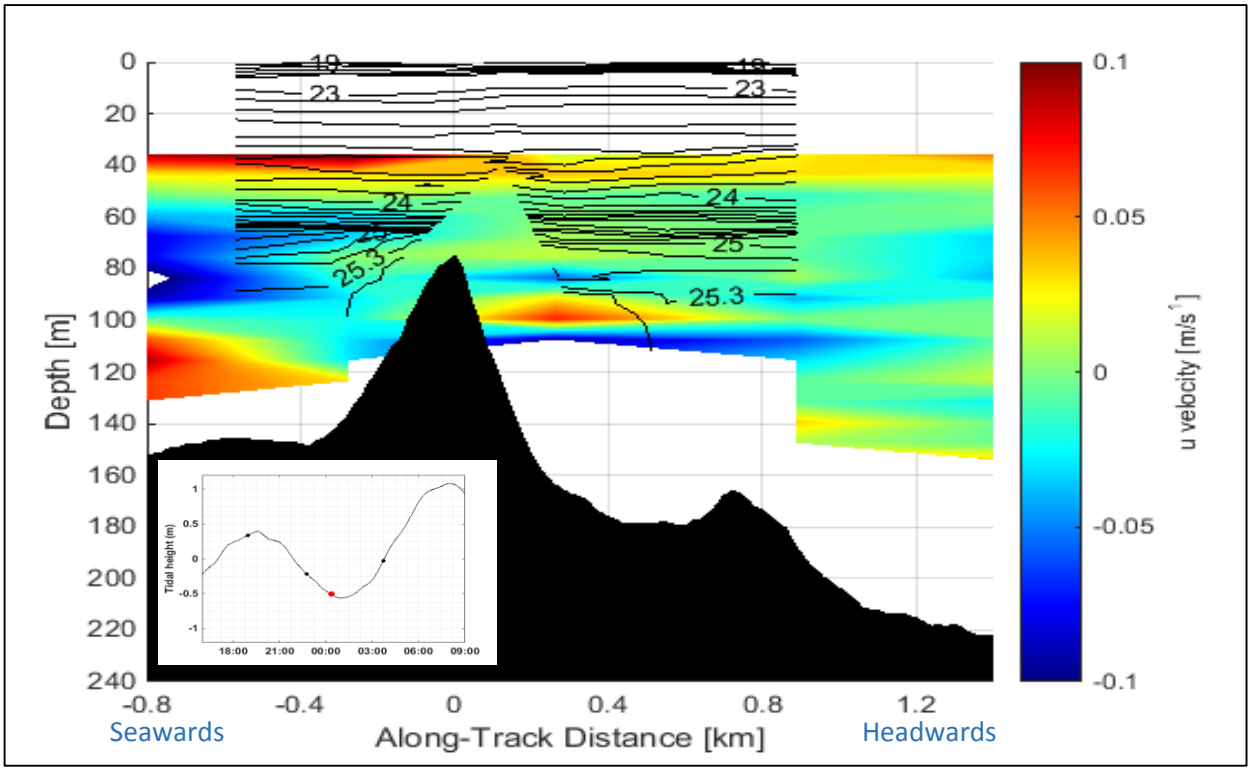

Figure 5(c): Williamson sill at slack water, before flood. The contour plot represents the velocity while the contour lines represent σ_t

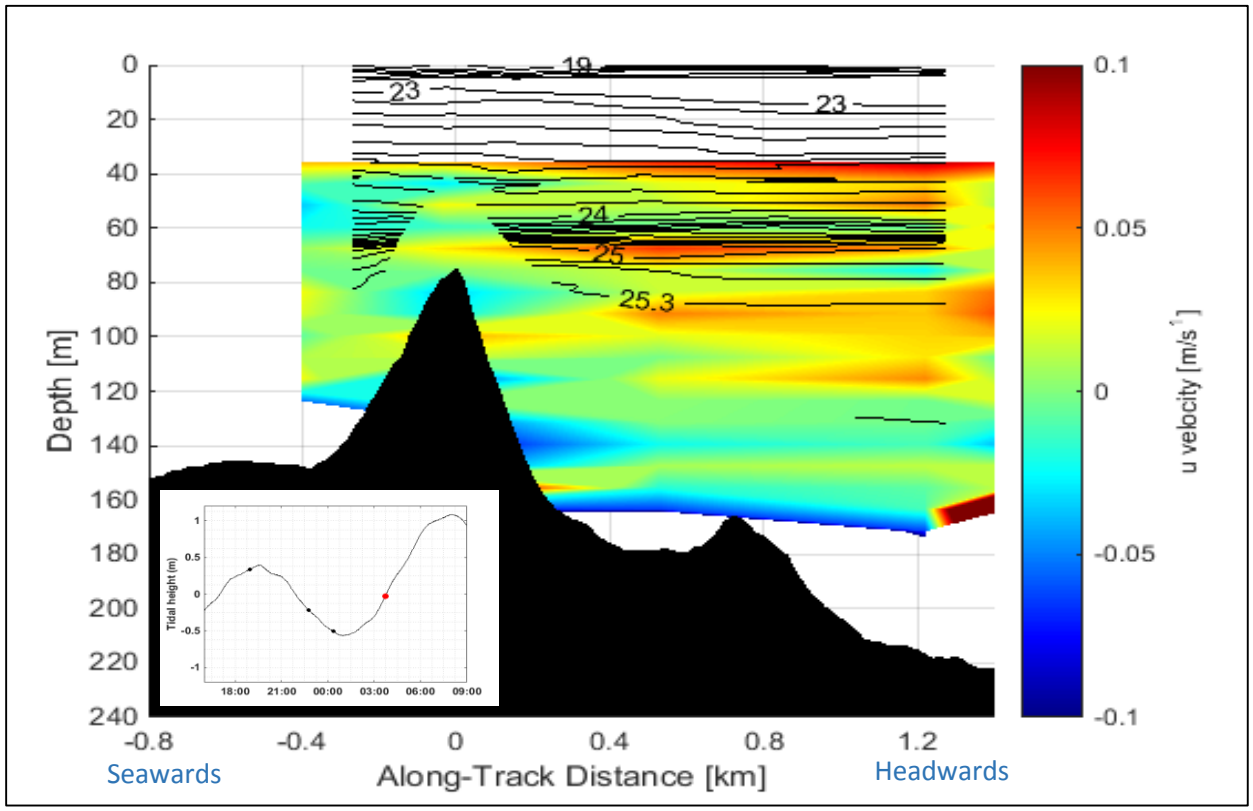

Figure 5(d): Williamson sill during flood. The contour plot represents the velocity while the contour lines represent σ_t

The general pattern shown by the isopycnals within the water column in Figure 5 is one whereby the isopycnal are at a shallower depth on the upstream side as compared to the downstream side. The near surface isopycnals (σ_t = 23kg/m^3) seem to pinch together on the upstream side of the sill and spread further apart on the downstream side of the sill during ebb (Figure 5(a)) and flood (Figure 5(c)). Figure 5(c) clearly shows the slight dipping of the isopycnals on either side of the sill.

Similar plots, with velocity over the different phases of the tidal cycle and contours of the vertical displacement (η) are represented. The red lines are representative of a negative vertical displacement (for example the isopycnals are deeper than the average level) while the black lines represent a positive vertical displacement (for example the isopycnals are

raised upwards). The contour interval of η is 2m and the bold black lines represent areas with zero vertical displacement.

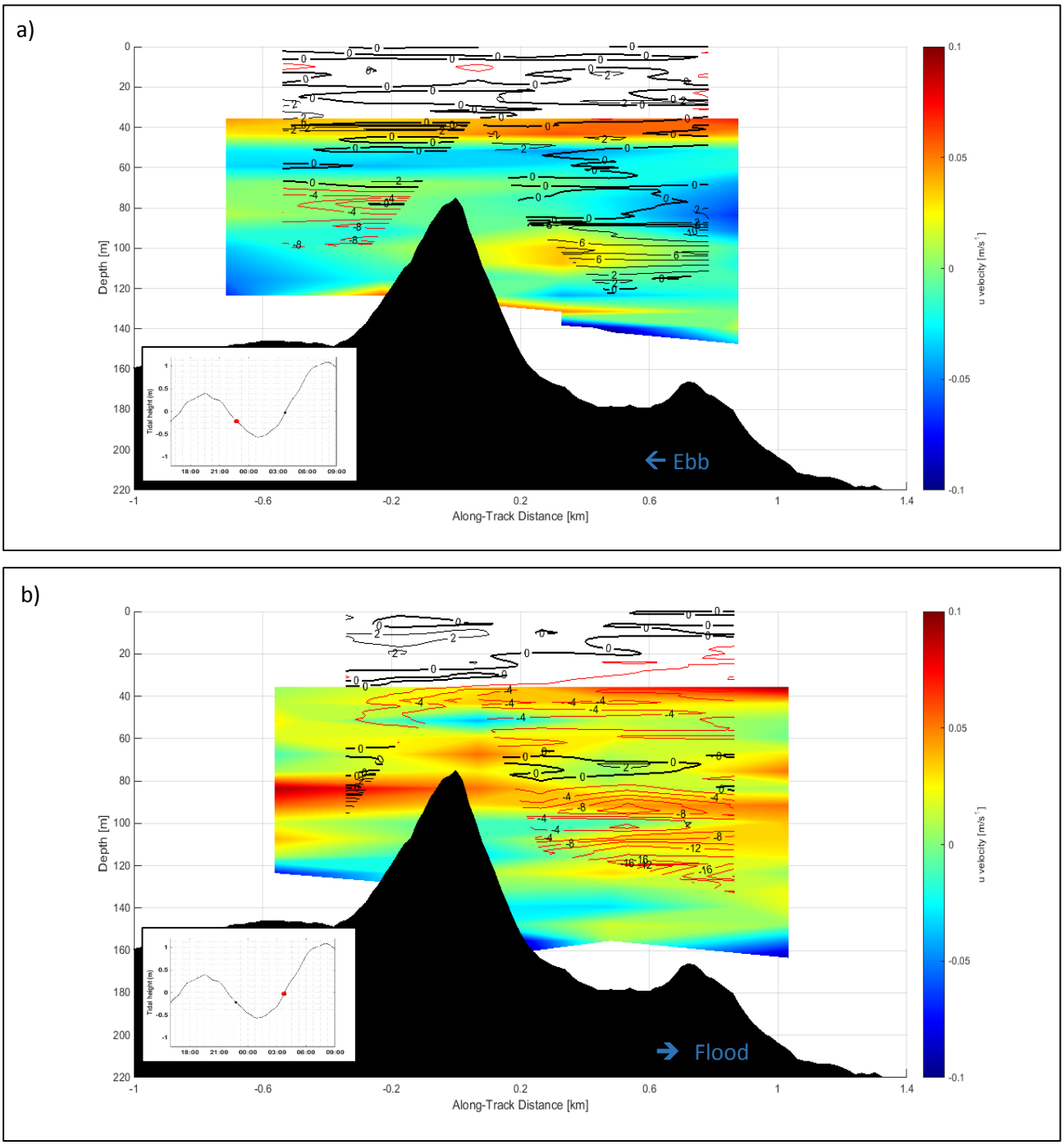

Figure 6: Vertical displacement (η) of isopycnals in meters. a) η during ebb and b) η during flood. The red lines represent negative vertical displacement while the black lines represent positive vertical displacement.

The vertical displacement is negative downstream of the sill and positive upstream in both cases of ebb (Figure 6(a)) and flood (Figure 6(b)). Furthermore, the displacement seems to be larger at depths greater than 60m. Several of these plots (one plot for each transect) were computed but only these two are presented in Figure 6 due to their similarity (that is downward displacement downstream and upward displacement upstream). However, two to three of the contour plots contained a mixture of both positive and negative vertical displacement when considering one side of the sill. One of these plots is shown below (Figure 7); the transect was done towards the end of the ebb and hence the vertical displacement represented is on the upstream side of the sill. The alternate upward and downward displacement with depth indicates the presence of an internal wave, which will be further discussed in the next section.

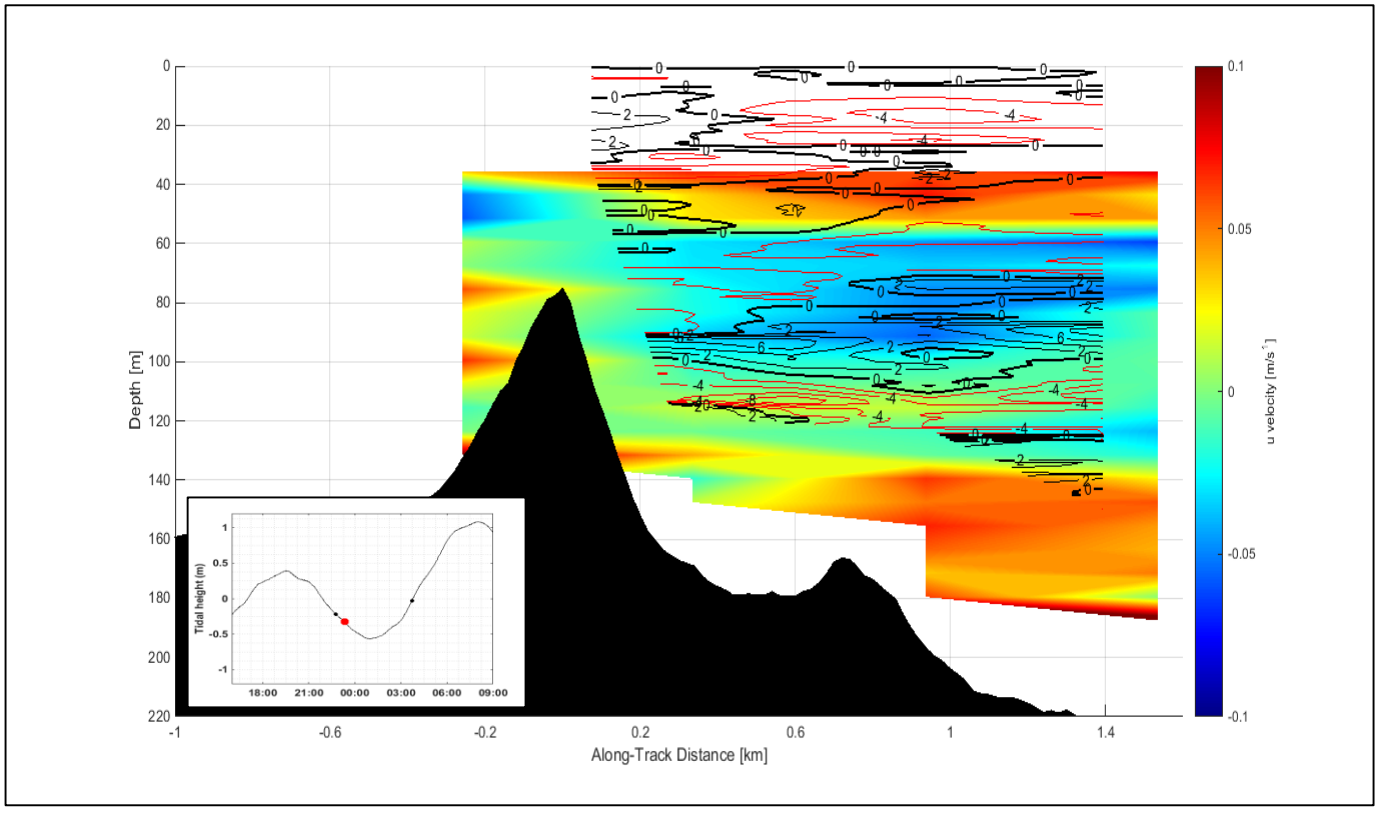

Figure 7: Vertical displacement (η) of isopycnals in meters on top of horizontal velocity towards the end of the ebb tide. The red lines represent negative vertical displacement while the black lines represent positive vertical displacement.

The velocity data from the ADCP and the density field given by the UCTD casts were used for an approximation of the Richardson Number at different phases of the tide as shown in Figure 8. Each subplot of Figure 8 contains its corresponding tidal chart to indicate which casts (over the tidal cycle) were taken into account for the plot. Figure 8 is a graph of the Buoyancy frequency to the square ($N^2 = -\frac{g}{\rho}\left(\frac{\partial \rho}{\partial z}\right)$) against the shear to the square ($S^2 = \left(\frac{\partial u}{\partial z}\right)^2$), the ratio of which is the Richardson number. Each subplot also contains two red lines delimiting areas with different Ri

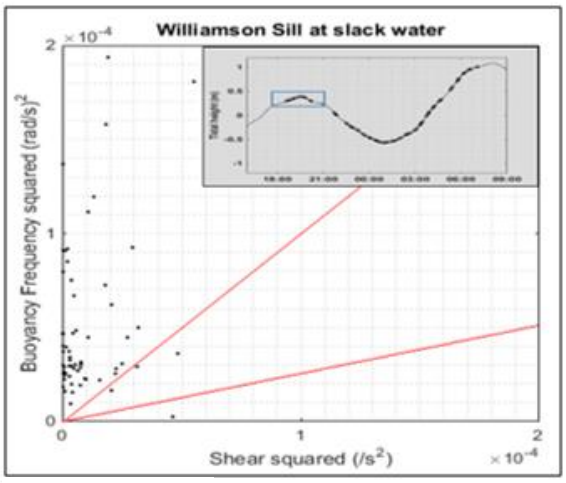

Figure 8 (a)

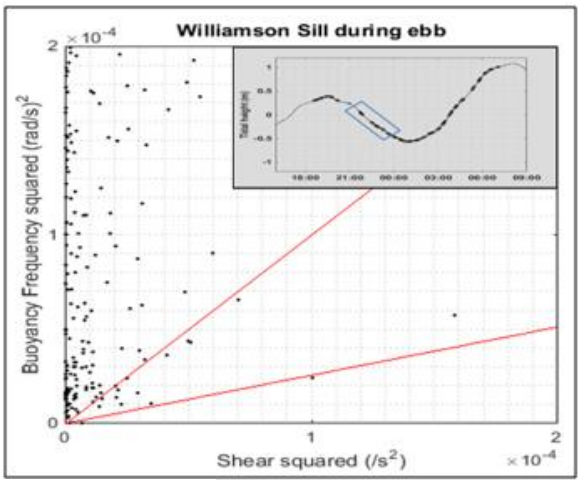

Figure 8 (b)

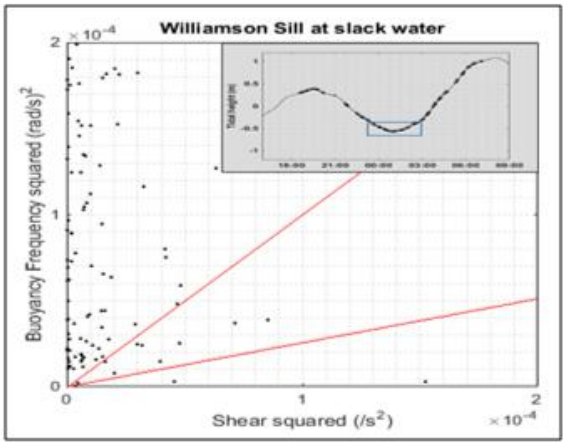

Figure 8 (c)

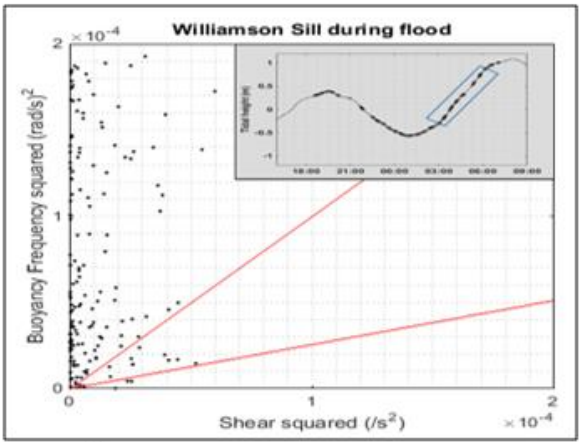

Figure 8 (d)

Figure 8: Plots of the buoyancy frequency to the square against the shear to the square. The section between the x-axis and the lower red line indicates Ri < 0.25, the section between the two red lines represents 0.25 < Ri < 1 and the section between the y- axis and the upper red lines specifies Ri > 1.

number. The section of the graph between the x-axis and the red line is representative of Ri < 0.25, indicating that the scatter in this plot area represent turbulent water. The section between the two red lines indicate 0.25 < Ri < 1 and hence represent water current in the transitional phase from laminar to turbulent while the section of the graph between the y-axis the red line represent Ri > 1; the water flow is laminar.

Considering the transitional phase from laminar to turbulent section in the subplots of Figure 8, there seems to be more markers (black dots on the plot) during the ebb and relatively less during the slack water phase before the start of the ebb. It is also important to note that there is nearly no marker in the turbulent section of the plot, with the water being mostly laminar in all the subplots due to the relatively small shear.

Figure 9 shows the location of these nearly turbulent water flows (represented in Figure 5) in the water column and their relative position to the sill. The circles represent Ri < 0.25 while the plus signs indicate 0.25 < Ri < 1 and the different colors of the markers refer to different times over the tidal phase. The line at the 35m depth indicate where the ADCP started recording velocity data, and hence at the upper 35m of the water column, no Richardson number could be calculated. It can be determined that the turbulence spans mostly at depths greater than 80m, with most of the turbulence being on the riverine side of the sill. The turbulence on the seawards side of the sill only occurred during the slack phase before the flood and during the flood period.

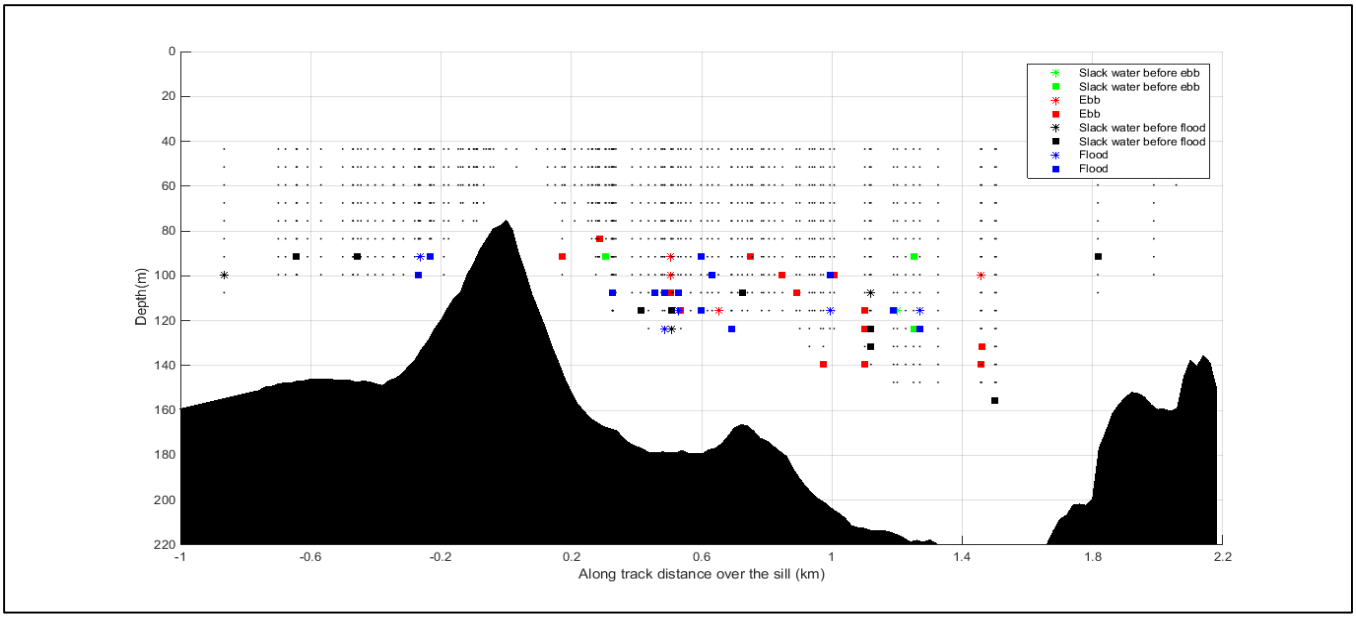

Figure 9: Location of turbulent flows across the water column. Stars represent Ri < 0.25, squares indicate 0.25 < Ri < 1 and the small dots represent Ri > 1

Discussion

Temperature inversion and stable boundary layer

Temperature maxima (Figure 1(a)) at depths is quite common in fjord. In fact, strongly developed maximum can be considered as a conservative feature at intermediate depths of the water column. The maxima's rate of erosion is a measure of the water replacement pattern near the fjord mouth (Gilmartin 1962). The Williamson sill most probably separates two water masses, a dense one with seawater properties and a fresher less dense one from the riverine discharge. Saline warm water is introduced into the fjord by the flooding tide at a depth of 75m, corresponding to the sill depth. Since the water mass from the ocean is denser, it will tend to sink beneath the surface riverine water lying on top. In winter, continuous cooling processes in the form of convective and turbulent transfer produces isothermal conditions from the surface to the bottom, with minimum temperature at the surface and maximum temperature at intermediate depths. The maxima persists if the cooling processes at the surface in winter is not strong enough

to reach the maxima at depths. Furthermore, mixing processes due to the interaction of the tidal flow with the sill, does not have any effect on the maxima since the turbulence generation zone lies below the 80m depth (Figure 6) and the temperature maxima is at about 55m. This will be further discussed later in the paper.

Considering the stability of the water column, hence the buoyancy frequency profile (Figure 1(d)), there is a peak at the 65m which can be interpreted as a second stable boundary layer at depth. Stability is directly proportional to the vertical density gradient which is mainly controlled by salinity and to a minor extent by temperature (Gilmartin 1962). However, in the present case the steep thermocline from 50 to 80m depths is more likely determining the pycnocline at 60m and the corresponding stable boundary layer at the same depth.

Evolution of the barotropic tidal flow over sill

Considering the contour plots for σ_t (Figure 5), there is an absence of the plunging jet and the entrainment interface as described by Farmer and Armi (1999) and shown in Figure 1. Further proof that the 'plunging jet' theory is not applicable in Williamson Sill is that there is no expansion of the intermediate mixed layer at any moment over the tidal cycle. Following Farmer and Armi (1999), the stagnant intermediate layer lies at about 20m above the sill crest and considering the plots in Figure 5, there is no significant spreading of the isopycnals at that depth. In fact, the stratification within the fjord plays a key role in the formation of the nearly stationary, adjusting lee depression; for this feature to be generated, a very distinct and pronounced pycnocline is required (Vlasenko et al. 2002). In Knight Inlet, British Columbia, where this 'plunging jet' mechanism was observed, the very stable boundary layer correlated

with the season of large freshwater runoff (spring and summer in this case),(Cummins et al. 2003). Conversely, as mentioned above, Muchalat Inlet experiences the maximum freshwater input in winter and from Figure 4(d), the contribution of the freshwater input leads to a buoyancy frequency of $0.09s^{-1}$ at the surface. While this value usually allow for the 'plunging jet' mechanism in some sills (Vlasenko et al. 2002), other factors also come into play, namely; the gradient of the slopes of the sill and the strength of the tidal current.

On the other hand, the 'lee waves' mechanism can be used to characterize the interaction of the tidal flow over the sill in this study. As explained by Nakamura et al. (2000), when the barotropic current flows over the sills, it produces upward fluxes on the upstream side of the sill and downward fluxes on the downstream side. These vertical flows in turn raise the isopycnals on the upstream side and depress them on the downward side of the sill. This statement holds true for the plots in Figure 6, where the positive vertical displacement is upstream and the negative vertical displacement lies downstream of the tidal current. Moreover, following the processes defining the 'lee wave' mechanism; as the tide slackens and the tidal ebb currents start to wane, internal lee waves are seen on the upstream side of the sill. This feature is clearly demonstrated through Figure 7, where the vertical displacement on one side of the sill involves intermittent vertical negative and positive displacement, characteristic of a propagating internal wave.

Internal lee waves

In order to confirm that the feature shown by Figure 7 is an internal wave, the vertical displacement (η) is shown with the shear (U_z) of the water column (Figure 10(a)). Following Gill (1982), for an internal wave, U_z is inversely correlated with η and when η is zero, U_z is

maximum in magnitude (when η is maximum, U_z is zero). This feature holds true for Figure 10(a), where negative displacement (brown contour lines) lie on top of the positive shear and the positive displacement (black contour lines) on top of the negative shear. The neutral displacement (bold black lines) are close to regions with high shear. Figure 10(b) is a schematic diagram that reproduces the direction of the main shear and the vertical displacement in Figure 10(a). The schematic diagram is compared to the Figure 11 from Gill (1982) that shows the phase and energy propagation of the internal waves as a function of density perturbations and velocity. The dashed lines indicate maximum (heavy) density perturbation; η > 0 and minimum (light) density perturbation; η < 0. The solid lines marks high pressure (maximum velocity) and low pressure (minimum velocity). Figure 10 (b) shows the same pattern as Figure 11 except for a reversal in the direction of motion. This implies that the direction of phase propagation is reversed (Gill, 1982) in Figure 10 (b); the phase propagation of the internal waves is directed

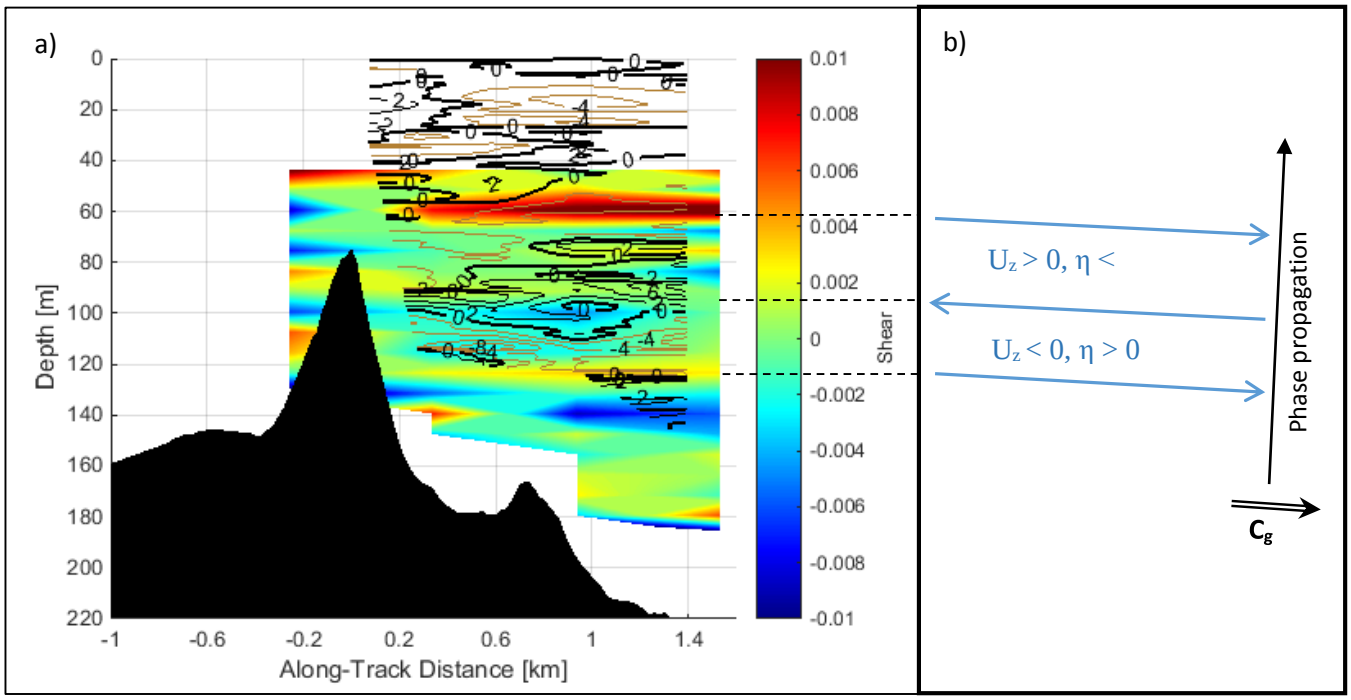

Figure 10: (a) represents the vertical displacement (η) on top of shear (U_z). The black contour lines represent upward displacement and the brown contour lines downwards displacement. (b) is a schematic diagram of the right panel and reproduces the main shear and vertical displacement within the water column, which is subsequently used to find the phase propagation direction.

upwards and their group velocity is to the right. The waves propagate up- fjord, away from the sill. These properties are coherent with the lee waves that are generated by tidal flow over the sill and held stationary at the downstream side. When the tidal currents start to fade away, the lee waves have a higher phase velocity, acquired during the maximum tidal flow, and can therefore propagate upstream.

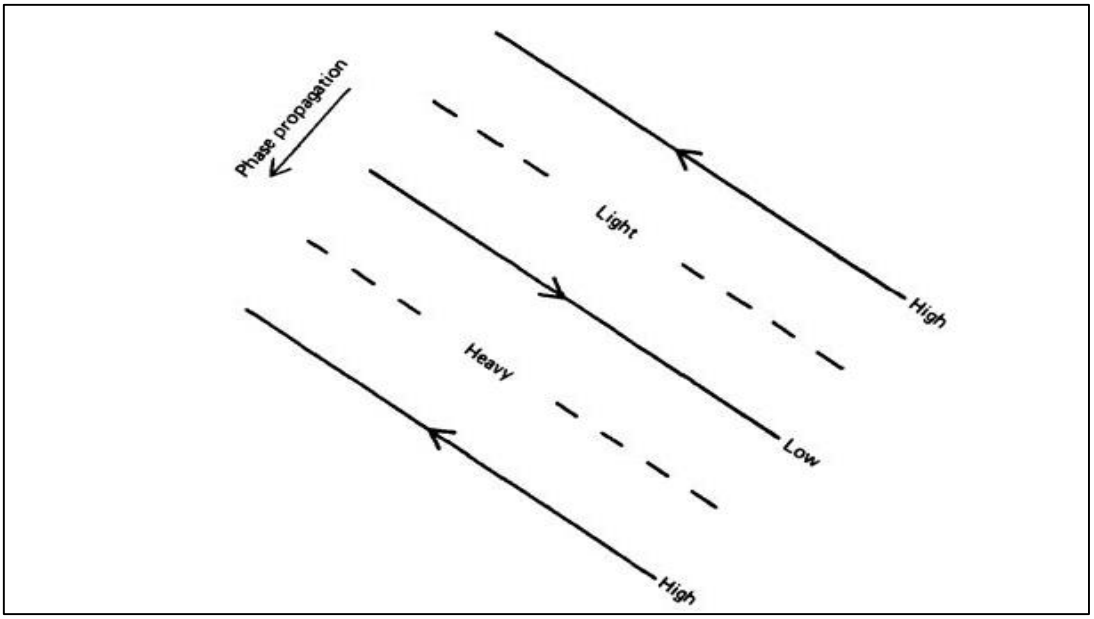

Figure 11: Schematic diagram from Gill (1982).” The solid lines mark lines of maximum (High) and minimum (Low) pressure, which are also lines of maximum and minimum velocity, the direction of motion being as shown. The dashed lines mark the positions of maximum (Heavy) and minimum (Light) density perturbations. If the direction of phase propagation is reversed, the only change is in the diagram is a reversal of the direction of motion.”

The vertical wavenumber of the internal lee wave can be calculated using the horizontal average of the vertical shear, vertical displacement and the buoyancy frequency throughout the water column. Simplifying the two equations for the dispersion relation of internal waves.

$$\frac{\eta}{U_z} = \frac{\sigma^2 - f^2}{kN^2}$$

$$\frac{m^2}{k^2} = \frac{N^2}{\sigma^2 - f^2}$$

The vertical wavenumber (m) is given by $\frac{1}{-N\left(\frac{\eta}{U_z}\right)}$ and was plotted in Figure 12(b). The pattern of the graph in Figure 12 correlates roughly with the one in Figure 13, whereby the horizontal mean of the vertical shear (U_z) was plotted against depth. The similar pattern between the two graphs further proves the presence of an internal wave at the upstream side of the sill in towards the end of the ebb. Based on Figure 12, the vertical wavelength (λ_z) of the internal wave is within the range of 25 to 30m.

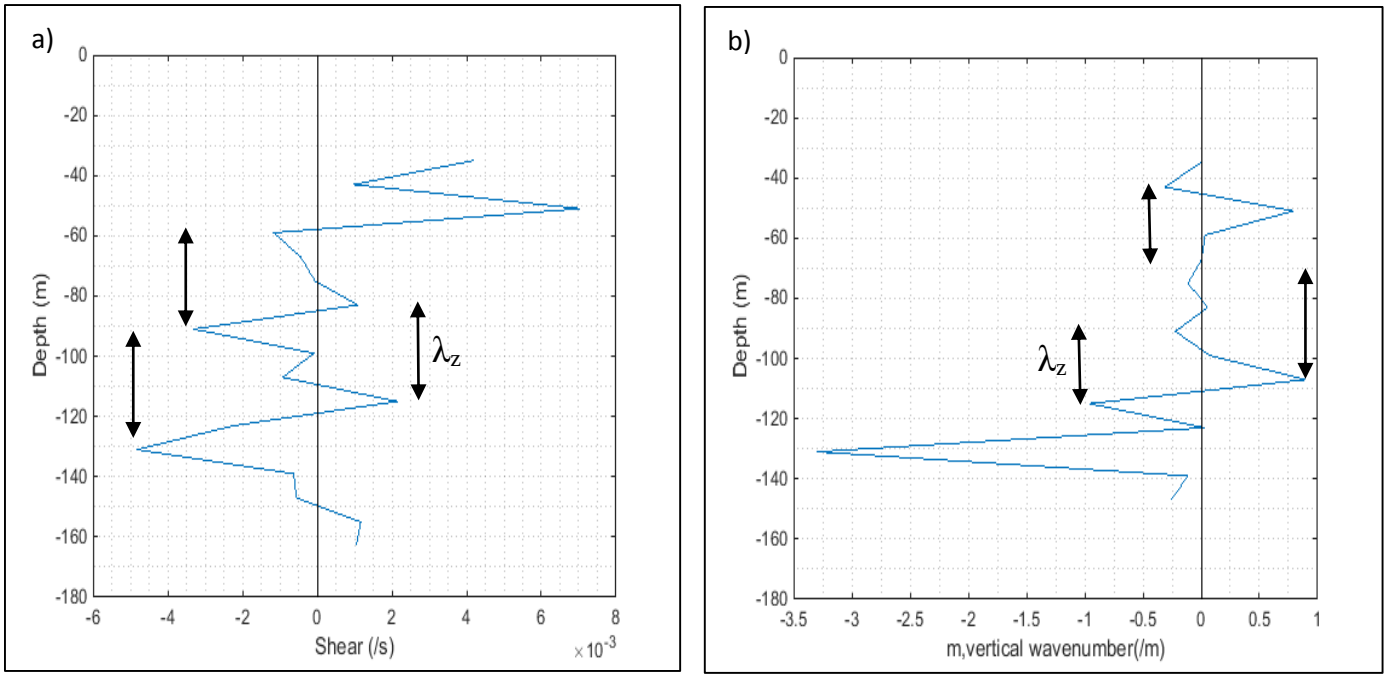

Figure 12(a) shows the corresponding mean vertical shear for the internal wave shown in Figure 8. Figure 12 (b) shows the calculated vertical wavenumber from the vertical shear, buoyancy frequency and vertical displacement. The black arrows on both panel indicate the vertical wavelength which is in the range of 20 to 30m

Turbulence and mixing

From Figure 1(d), there are two well mixed layers on either side of the weaker stably stratified layer at 65m depth. The buoyancy frequency at depths 50m to 80m is high enough to overcome the destabilising effect of the vertical shear and turbulence, generated either at the surface or at depths below the pycnocline. The lower well mixed region correlates well with the layer of low

Richardson number that is at depths greater than 80m (Figure 9). Figure 8 shows fluctuations in the number of instances for low Richardson Number within the water column as the tidal flow evolves. These changes in Ri indicate a variation in the intensity of mixing and hence demonstrate that the turbulent dissipation rate is modulated over the tidal cycle. It also implies that the source of mixing for the lower mixed layer is internal waves while the upper mixed layer might be sustained by wind- generated motions. In this case, wind-generated motion propagate downwards from the surface but is contained within the 45m surface water by the sub- surface stably stratified layer. Due to the limitation of the ADCP, it cannot be confirmed if the upper mixed layer experiences turbulent flow but the low buoyancy frequency from 20m to 50m (Figure 1) is a good approximation of turbulence. The upwards phase propagating internal waves generated at the sill are not constrained but are refracted at the sub- surface stably stratified layer. In this case, the layer is stable enough to withstand the turbulence generated by the interference of two such propagating wave.

Figure 8 shows that there is generally more turbulence during the ebb and flood as compared to slack water. This corresponds to the generation and propagation mechanism of lee interval waves. The waves are generated during the first half of the flood (or ebb) and propagate away as the tidal current starts to fade away; hence the large number of low Ri. At slack, there is not much turbulence since the internal wave already started to propagate upstream, away from the sill area. The reversing tidal current can carry the lee waves away from the sill.

Conclusion

The extent of this study and the data acquired allowed the identification of internal lee waves as a result of tidal flow over Williamson Sill, in Nootka Sound, British Columbia. However, there

were some limitations that prevented further characterisation of the waves generated at the sill. For instance, the surface velocity was not available; velocities below the 40m depths are minimal in comparison to surface velocities and hence have a minor contribution to the depth mean velocity. Further study at Williamson Sill should consider the measurement of the surface velocity and will therefore allow the calculation of the densimetric Froude Number which gives the criticality of the flow. The densimetric Froude Number can subsequently indicate the occurrence of a hydraulic jump that triggers significant mixing within the water column. The surface velocities would also allow the computation of the average turbulent kinetic energy dissipation rates and hence help in the quantification of the mixing events that result from the internal lee waves.

References:

Buijsman MC, Kanarska Y, McWilliams JC (2010) On the generation and evolution of nonlinear internal waves in the South China Sea. J Geophys Res 115:1–17.

Carter GS, Gregg MC, Lien RC (2005) Internal waves, solitary-like waves, and mixing on the Monterey Bay shelf. Cont Shelf Res 25:1499–1520.

Da Silva JCB, Buijsman MC, Magalhaes JM (2015) Internal waves on the upstream side of a large sill of the Mascarene Ridge: a comprehensive view of their generation mechanisms and evolution. Deep Sea Res Part I Oceanogr Res Pap 99:87–104Description G, Processes

Farmer DM, Howard FJ (1983) The Physical Oceanography of Fjords. Prog Oceanogr 12:147–220.

Farmer DM, Dungan Smith J (1980) Tidal interaction of stratified flow with a sill in Knight Inlet. Deep Sea Res Part A Oceanogr Res Pap 27:239–254

Finnigan TD, Luther DS, Lukas R (2002) Observations of Enhanced Diapycnal Mixing near the Hawaiian Ridge. J Phys Oceanogr 32:2988–3002.

Garrett C, Kunze E (2007) Internal Tide Generation in the Deep Ocean. Annu Rev Fluid Mech 39:57–87.

Gill AE (1982) Atmosphere- Ocean dynamics. Elsevier.

Hibiya T (1990) Generation mechanism of internal waves by a vertically sheared tidal flow over a sill. J Geophys Res 95:1757.

Ivey GN, Winters KB, Koseff JR (2008) Density Stratification, Turbulence, but How Much Mixing? Annu Rev Fluid Mech 40:169–184

Klymak JM, Moum JN (2007) Oceanic Isopycnal Slope Spectra. Part II: Turbulence. J Phys Oceanogr 37:1232–1245

Kunze E, Rosenfeld LK, Carter GS, Gregg MC (2002) Internal Waves in Monterey Submarine Canyon. J Phys Oceanogr 32:1890–1913.

Lamb KG (2004) On boundary-layer separation and internal wave generation at the Knight Inlet sill. Proc R Soc A Math Phys Eng Sci 460:2305–2337.

Maxworthy T (1979) A note on the internal solitary waves produced by tidal flow over a three-dimensional ridge. J Geophys Res 84:338.

Nakamura T, Awaji T, Hatayama T, et al (2000) The Generation of Large-Amplitude Unsteady Lee Waves by Subinertial K 1 Tidal Flow: A Possible Vertical Mixing Mechanism in the Kuril Straits. J Phys Oceanogr 30:1601–1621.

Nakamura T, Isoda Y, Mitsudera H, et al (2010) Breaking of unsteady lee waves generated by diurnal tides. Geophys Res Lett 37:1–5

Polzin K (2014) Journal of Geophysical Research : Oceans Finescale parameterizations of turbulent dissipation. 1383–1419.

Ross L, Perez-Santos I, Valle-Levinson a., Schneider W (2014) Semidiurnal internal tides in a Patagonian Fjord. Prog Oceanogr 129:19–34.

Stewart KD, Hughes GO, Griffiths RW (2011) When do marginal seas and topographic sills modify the ocean density structure? J Geophys Res Ocean 116:1–15.

Van Haren H (2005) Internal waves near the buoyancy frequency in a narrow wave-guide. J Sea Res 53:121–129.

Vlasenko V, Stashchuk N, Hutter K (2002a) Water exchange in fjords induced by tidally generated internal lee waves. Dyn Atmos Ocean 35:63–89.

-